Biomechanical analysis of Combi-hole locking compression plate during fracture healing

Li, Zeyang; Pollard, Stuart; Smith, Gemma; Deshmukh, Subodh; Ding, Ziyun

Biomechanical analysis of Combi-hole locking compression plate during fracture healing: a numerical study of screw configuration

Journal:	*Part H: Journal of Engineering in Medicine*
Manuscript ID	JOEIM-23-0211.R1
Manuscript Type:	Original article
Date Submitted by the Author:	20-Dec-2023
Complete List of Authors:	Li, Zeyang; Cardiff University Pollard, Stuart; University of Birmingham Smith, Gemma; Royal Orthopaedic Hospital Deshmukh, Subodh; Sandwell and West Birmingham Hospitals NHS Trust Ding, Ziyun; University of Birmingham, School of Engineering
Keywords:	Finite Element [Biomechanics], Bone Biomechanics, Bone Remodelling, Implants/ Prosthetics, Finite Element Modelling/ Analysis [Medical]
Abstract:	Background: Locking compression plates (LCPs) have become a widely used option for treating femur bone fractures. However, the optimal screw configuration with combi-holes remains a subject of debate. The study aims to create a time-dependent finite element (FE) model to assess the impacts of different screw configurations on LCP fixation stiffness and healing efficiency across four healing stages during a complete fracture healing process. Methods: To simulate the healing process, we integrated a time-dependent callus formation mechanism into a FE model of the LCP with combi-holes. Three screw configuration parameters, namely working length, screw number, and screw position, were investigated. Results: Increasing the working length negatively affected axial stiffness and healing efficiency ($p < 0.001$), while screw number or position had no significant impact ($p > 0.01$). The time-dependent model displayed a moderate correlation with the conventional time-independent model for axial stiffness and healing efficiency ($\rho \geq 0.733$, $p \leq 0.025$). The highest healing efficiency (95.2%) was observed in screw configuration C125 during the 4-8-week period. Conclusions: The results provide insights into managing fractures using LCPs with combi-holes over an extended duration. Under axial compressive loading conditions, the use of the C125 screw configuration can enhance callus formation during the 4-12-week period for transverse fractures. When employing the C12345 configuration, it becomes crucial to avoid overconstraint during the 4-8-week period.

Biomechanical analysis of Combi-hole locking compression plate during fracture healing: a numerical study of screw configuration

Zeyang Li[1], Stuart Pollard[2], Gemma Smith[3], Subodh Deshmukh[3], Ziyun Ding[2]*

1. School of Engineering, Cardiff University, Cardiff, UK
2. School of Engineering, University of Birmingham, Birmingham, UK
3. Royal Orthopaedic Hospital, Birmingham, UK

Correspondence:

Ziyun Ding

School of Engineering

University of Birmingham

Birmingham

UK

B15 2TT

z.ding@bham.ac.uk

Abstract

Background: Locking compression plates (LCPs) have become a widely used option for treating femur bone fractures. However, the optimal screw configuration with combi-holes remains a subject of debate. The study aims to create a time-dependent finite element (FE) model to assess the impacts of different screw configurations on LCP fixation stiffness and healing efficiency across four healing stages during a complete fracture healing process. Methods: To simulate the healing process, we integrated a time-dependent callus formation mechanism into a FE model of the LCP with combi-holes. Three screw configuration parameters, namely working length, screw number, and screw position, were investigated. Results: Increasing the working length negatively affected axial stiffness and healing efficiency ($p < 0.001$), while screw number or position had no significant impact ($p > 0.01$). The time-dependent model displayed a moderate correlation with the conventional time-independent model for axial stiffness and healing efficiency ($\rho \geq 0.733$, $p \leq 0.025$). The highest healing efficiency (95.2%) was observed in screw configuration C125 during the 4-8-week period. Conclusions: The results provide insights into managing fractures using LCPs with combi-holes over an extended duration. Under axial compressive loading conditions, the use of the C125 screw configuration can enhance callus formation during the 4-12-week period for transverse fractures. When employing the C12345 configuration, it becomes crucial to avoid overconstraint during the 4-8-week period.

44 **Keywords***:* screw configuration; fracture healing; finite element; callus; locking compression plate

1. Introduction

The use of locking compression plates (LCP) in plate osteosynthesis is a significant advancement. In comparison to conventional plates, such as dynamic compression plates (DCP), LCPs offer several advantages in reducing the risk of biological complications, including infection and non-union.[1,2] This is achieved through indirect reduction that avoids direct bone-implant contact, promoting relative stability rather than absolute stability. The non-contact features of LCPs contribute to optimal healing and biological callus formation, with factors such as axial stiffness and inter-fragmentary movement (IFM) being crucial to the process.[3,4] Proper levels of axial stiffness and IFM are beneficial to healing,[5-9] but excessive or insufficient levels can be detrimental and even cause non-union. Therefore, achieving the optimal trade-off between these mechanical variables is essential for successful healing.[10-13.]

LCPs with combi-holes, which combine conventional and threaded holes, provide versatility and flexibility by accommodating both conventional and locking head screws. However, this introduces uncertainty that requires careful consideration of the biomechanical implications of different screw configurations. Although previous biomechanical studies have mainly investigated the effects of screw configurations, none have analysed the use of LCPs with combi-holes.[9-16] Therefore, it is important to investigate the mechanical properties of LCPs with combi-holes to determine the most effective screw configurations and optimize their clinical use.

During the fracture healing process, bone and soft tissues undergo continuous changes in shape and material properties, posing a challenge in determining the optimal screw configurations. Numerical finite element (FE) modelling has shown promise in simulating this healing process. For example, Gardner et al. simulated the formation of callus tissue successfully and calculated the Young's modulus of callus at different healing stages[17]; expanding upon Gardner's works, Kim developed a time-dependent callus model to investigate the influence of the plate materials on tibia DCP fixation stiffness[18]; building on this research, Mehboob et al. used a stress-based rejection coefficient algorithm to calculate callus properties during the healing process.[19] However, these studies focused primarily on healing simulation or were limited to a DCP system, making them incapable of investigating the effects of different screw configurations in an LCP system over an extended duration.

This study aims to develop a finite element modelling framework for simulating callus growth during the fracture healing process. To achieve this, a time-dependent callus model was incorporated into an FE model of the bone-implant construct. Three configuration parameters, namely the working length (WL), screw number (SN) and screw position (SP) were investigated to assess the quantitative impact of screw configuration on fracture healing under given loading conditions. We hypothesised that the screw configuration affects mechanical variables, specifically, axial stiffness and interfragmentary strain (IFS), which were known to influence healing efficiency. This information can provide insights into managing fractures at different stages based on the selection of screw configurations for LCP plates with combi-holes. Such consideration may potentially contribute to improved healing efficiency throughout the entire healing process.

2. Methods and materials

2.1 The bone-implant construct

A standardised LCP with ten combi-holes (VP4031, APLUS BIOTEC Ltd) and locking screws (LS5034, APLUS BIOTEC Ltd) was modelled using Solidworks 2020 (DS Solidworks Copr., USA), as illustrated in Figure 1a. The LCP had dimensions of 150 mm length, 10 mm width, and 4 mm thickness, with an 11 mm distance between adjacent combi-holes. The locking head screw had a length of 34 mm, an inner diameter of 7.2 mm, an external diameter of 5 mm and a shaft diameter of 4.3 mm.

(Insert Figure 1)

To construct the bone-implant model, the contour of femoral cortical bone was derived from magnetic resonance imaging (MRI) scans of a healthy male subject (age: 44 years, height: 1.84 m, weight: 96 kg) using Mimics (Mimics 19.0, Materialise, Belgium). The average cross-sectional area was 103.9 mm^2 and the cortical thickness was 3.5 mm, as shown in Figure 1b. It was then extruded longitudinally to a length of 140 mm to construct the three-dimensional shape. To enhance computational efficiency, this work excluded the trabecular structure.[19,21] In addition, to simulate a 32-A3 femoral shaft fracture, a transverse gap of 2.1 mm was created in the middle of the cortical bone. The transverse fracture introduces symmetry along the fracture gap, and the size of the transverse gap is consistent with previous studies, within the range of 2 mm to 5 mm.[7-9,22] In the context of midshaft transverse fracture, previous studies also indicated the limited impact of the bone length.[18,25,31]

A time-independent FE model was created using ABAQUS (2020, Dassault Systèmes, USA). The model incorporated a 2 mm offset between the bone and plate, and symmetry along the longitudinal axis, effectively reducing computational cost.[23] The screw-bone and screw-plate interfaces were represented as tied. One end of the bone was fixed, while the other end was subjected to a compressive load of 1053.6 N, equivalent to 1.12 times the body weight of the subject.[24] The LCP plate and screws were made of homogeneous and isotropic Titanium alloy (Ti–6Al–4V) and cobalt-based superalloy, respectively. The cortical bone was anisotropic. Table 1 provides detailed information on the material properties.

(Insert Table 1)

The screws and cortical bone were meshed using an 8-node linear hexahedral solid element with reduced integration (C3D8R), while the plate was meshed using a tetrahedron element (C3D4).[4] A mesh convergence analysis was performed iteratively until the maximum stress change was less than 2% with decreasing mesh size.[20] A smaller mesh size of 0.15 mm was required at the tied interfaces, reducing the maximum stress from 10.4% to 1.5% (Figure. 1c). The remaining part had an average size between 0.5 mm to 0.7 mm. The model consisted of approximately 50,000 and 572,000 hexahedral elements for the screws and bone, and 725,600 tetrahedron elements for the plate.

2.2 A time-dependent model

In addition to the time-independent model described in Section 2.1, a time-dependent model was proposed by modelling the callus tissue, which possesses time-dependent material properties in different healing stages [18,25,28]. Only the central component of the callus was modelled as it provides the primary load-bearing capacity and is the most sensitive to the IFM.

According to the interfragmentary strain theory,[29] callus growth can be determined by interfragmentary strain (IFS, ε): an IFS between 2-10% promotes callus growth, while an IFS below 2% or above 10% inhibits it.[18,30] IFS was calculated as the displacement of the fracture gap divided by its original size (as illustrated in Figure 2b). The success of callus growth determines healing efficiency (δ), expressed as the ratio of A_c and A_t. A_c is the area with an IFS between 2-10% and A_t is the total fracture area (as illustrated in Figure 2b).

(Insert Figure 2)

In our study, we divided a complete healing process into four stages (i.e., 1-4 weeks, 4-8 weeks, 8-12 weeks and 12-16 weeks).[17] As a result, the Young's modulus of callus (E_n) during a particular healing stage (n) was estimated as follows:

$$E_n = \delta_{n-1} \cdot E_{standard,n} + (1 - \delta_{n-1}) \cdot E_{n-1} \quad (1)$$

where $E_{standard,n}$ represents the standard callus modulus and its values at four stages are outlined in Table 2. These values are determined under the condition where the healing efficiency (δ) is equal to 100%;[17] E_{n-1} is Young's modulus of the callus at the $(n-1)$ healing stage; δ_{n-1} is the healing efficiency at the $(n-1)$ healing stage, calculated from the FE model. The iterative calculation for the callus modulus is illustrated in Figure 2b. There are four layers of callus connecting the fracture gap along the axial direction, meshed using 8-node linear hexahedral solid elements with reduced integration (C3D8R) and a size of 0.5 mm. In total, there are 2852 elements.

The compressive loading conditions were varied in the time-dependent model to account for the mobility improvement after the operation (Table 2): during the initial two stages (1-4 weeks and 4-8 weeks), the compressive load was equal to 1.12 times body weight (BW);[24] in the third stage (8-12 weeks), the load was increased to 2 times BW, representative of walking with a walking-stick;[31] in the final stage (12-16 week), the load was raised to 3 times BW, representative of normal walking without a walking-stick.[31] The axial stiffness is defined as the axial compressive load divided by the displacement at the centre points of the two ends of the bone (as illustrated in Figure 1a).

2.3 Design of screw configurations

Different screw configurations were studied (Figure 3) by varying the working length (the distance between the closest screws on either side of the fracture, case 1), the number of screws (case 2), and the position of screws (case 3). For case 1 (C15, C25, C35, C45), the working length was increased with two screws. For case 2 (C15, C145, C1345, C12345) the screw numbers were increased with a constant working length. For case 3 (C125, C135, C145), the middle screw was positioned differently relative to the fracture gap with a constant screw number and working length. The fifth screw (the screw near the distal side) was tightened in each configuration to ensure an adequate torsion stiffness of fixation [4]. This resulted in nine different screw configurations, each tested under five scenarios: post-operation using the time-independent model; 1–4 weeks, 4-8 weeks, 8-12 weeks and 12-16 weeks using the time-dependent model. In total, 45 simulation scenarios were conducted.

(Insert Figure 3)

2.4 Data processing and analysis

Non-parametric repeated measure Friedman tests were employed to assess the differences in axial stiffness and corresponding healing efficiency in different healing stages. Post-hoc comparisons were then conducted using a Wilcoxon signed-rank test with Bonferroni correction. Furthermore, Spearman's correlation coefficient (ρ) was used to calculate any correlations in predicted stiffness and healing efficiency between the time-independent model and the time-dependent model. The strength of the correlations was categorized as poor ($\rho < 0.3$), fair ($0.3 < \rho < 0.5$), moderately strong ($0.6 < \rho < 0.8$), very strong ($0.8 < \rho < 1$), and perfect ($\rho = 1$). [36] All statistical analysis was performed with SPSS (R26, IBM co. ltd, US) with a significance level of $\alpha = 0.01$.

3. Result

The predicted axial stiffness using the time-independent model was compared with previous studies, as shown in Figure 4. Despite the variations in material properties and loading conditions, our estimations were within a reasonable range (between 713.1 N/mm and 836.8 N/mm), indicating that our model was capable of predicting LCP stiffness accurately.

(Insert Figure 4)

In the time-dependent model, Young's modulus of callus increased across four stages, resulting in a corresponding increase in axial stiffness (Figure 5). Notably, the configuration of C45 exhibited the lowest axial stiffness (Figure 6a). The predicted axial stiffness from the time-dependent model exhibited a significant correlation with that from the time-independent model (Figure 6c, $\rho \geq 0.733$, $p \leq 0.025$) as well as with the healing efficiency (Figure 6d, $\rho \geq 0.717$, $p \leq 0.030$).

(Insert Figure 5 and Figure 6)

The highest healing efficiency accompanied by a strain of less than 2%, was observed at 4-8 weeks post-operation (Figure 7). Among the configurations tested, C12345 exhibited the largest area of strain that is less than 2% (Table

3).

(Insert Figure 7, Table 3)

The working length had a significant effect on both axial stiffness and healing efficiency (*p*-adjust < 0.001). The addition of screws increased both the stiffness and healing efficiency, but its effect was not statistically significant (*p*-adjust ≥ 0.017 and *p*-adjust ≥ 0.024).

(Insert Figure 8)

4. Discussion

This study aimed to develop a finite element modelling framework for simulating callus growth during the fracture healing process, considering three configuration parameters: working length, screw number and screw position. According to clinical recommendations,[41] the C12345 configuration is commonly believed to provide the highest stiffness and stability. However, when comparing different configurations over an extended duration, our modelling framework revealed that C125 outperformed C12345 in terms of both stiffness and healing efficiency during weeks 4-12, despite using fewer screws. During the 4-8-week period, C12345 exhibited the largest area of strain that was less than 2%, potentially impeding callus growth and resulting in lower healing efficiency. This effect persisted until the 8-12-week period, as the reduced healing efficiency at the 4-8-weeks contributed to the reduced callus modulus at the later stage. This finding suggests that C125 may represent a more effective screw configuration for LCP fixation under the given conditions, as indicated by the higher mean healing efficiency of 75.3% when compared to the mean healing efficiency of 73.7% in C12345 between weeks 4-12.

This study provided novel insights into the relationship between stiffness and healing efficiency in the LCP with combi-holes during the healing process. Our time-dependent model revealed a significant, positive correlation between stiffness and healing efficiency in four different healing stages ($\rho \geq 0.717$)

highlighting the importance of achieving an optimal level of stiffness for promoting bone healing. Interestingly, our results showed that most of the screw configurations resulted in a "loose" fixation, as identified by the IFS greater than 10% (Figure 7). However, a moderate increase in fixation stiffness could increase the area of IFS between 2-10%, promoting callus growth and bone healing. This finding is consistent with the available literature, which suggests that increased compressive force can accelerate bone healing.[42,43] Moreover, our study indicates that weight-bearing activities after four weeks of operation could be an effective means of achieving this goal.

Our hypothesis that the screw configuration affects fracture healing was partially supported. We found that only the working length significantly affected healing efficiency (Figure 8, $p < 0.001$), while the effects of the screw number and position were not significant in the healing process (Figure 8). Our findings are in line with previous studies, which have indicated that using an excessive number of screws may not always result in improved healing efficiency.[44-46] While it is challenging to recommend a definite number of screws for LCP usage, it is advisable to anchor in the fragments proximal and distal to the fracture zone.[47] Our findings align with this recommendation, as C15 outperformed the others with the same number of screws in terms of axial stiffness and healing efficiency.

Our time-dependent callus modelling was based on the strain-driven mechanism in which a displacement index IFS was applied to calculate the material property of the callus. This approach differs from some modelling studies that have used a stress-driven mechanism.[48] Stress-driven models can be more susceptible to boundary conditions, and the strain-driven approach employed in this study could avoid contradictory results with previous studies. In the Appendix, the predicted stress pattern at the bone-callus interface was provided for comparison with the IFS strain pattern observed in previous studies.[18]

The study had several limitations that need to be considered when interpreting the results. Firstly, we only modelled one fracture scenario, namely the transverse fracture with a gap size of 2.1 mm. This established a baseline for the investigation of screw configurations. Additionally, only a limited set of screw configurations were modelled; other potential configurations, such as C1245, C2345, and C1235, were not considered. Importantly, it's worth noting that the relative differences between screw configurations are not expected to be influenced by the size of the transverse fracture gap. Secondly, our model only incorporated the central callus and excluded the peripheral and adjacent regions, which avoids geometric nonlinearity and convergence issues. However, this limitation may affect the predicted stiffness due to peripheral tissue differentiation during the healing process. Third, the study did not account for intra-operative variability, such as soft tissues and patient/surgeon factors, which may confound the theoretical findings. Fourth, our FE model solely accounted for the compressive force along the longitudinal direction of the femur and its increase at different healing stages, indicating improved mobility post-operation. However, it fails to adequately represent the physiological loading conditions as it overlooks thigh muscle contractions and shear from internal hip joint contact forces. These estimations pose computational challenges and are sometimes infeasible. Considering these limitations and modelling assumptions, we acknowledge that our results may not be directly transferable to clinical recommendations for patients. In clinical practice, significant variations exist among different fracture types and circumstances, both between patients and surgeons. However, our study leverages the advantages of numerical simulation to investigate the effects of screw configuration at different healing stages and their resulting influence on later stages, providing insights to enhance overall healing efficiency throughout the entire healing process, specifically for simple transverse fractures under axial loading conditions.

5. Conclusions

A novel time-dependent FE model was developed to assess the impact of screw configurations on the LCP fixation stiffness and healing efficiency throughout a complete fracture healing process. Under axial compressive loading conditions, our findings suggest that a decrease in the working length can effectively promote fixation stability and healing efficiency. The positive correlation between healing efficiency and axial stiffness also underscores the importance of using configurations with higher stiffness. However, it is important to note that during the 4-8-week post-surgery, configurations like C12345 may lead to overconstraint in bone motion. Overall, our study suggests that under axial compressive loading conditions, the use of the C125 screw configuration can enhance callus formation during the 4-12-week period for transverse fractures. The findings provide insights into managing fractures using LCPs with combi-holes over an extended duration, with the potential to improve healing efficiency.

Acknowledgements

Zeyang Li would like to thank the support of the China Scholarship Council for sponsoring his PhD project at Cardiff University.

Conflict of Interest

No benefits in any form have been or will be received from a commercial party related directly or indirectly to the subject of this manuscript.

References

1. Farouk O, Krettek C, Miclau T, et al. Effects of percutaneous and conventional plating techniques on the blood supply to the femur. *Arch Orthop Trauma Surg* 1998; 117: 438-441.

2. Hasenboehler E, Rikli D, and Babst R. Locking Compression Plate with Minimally Invasive Plate Osteosynthesis in diaphyseal and distal tibial fracture: A retrospective study of 32 patients. *Injury* 2007; 38: 365-370.

3. Duda N, Kirchner H, Wilke J, et al. A method to determine the 3-D stiffness of fracture fixation devices and its application to predict inter-fragmentary movement. *J Biomech* 1997; 31(3): 247-252.

4. MacLeod A, Simpson AH and Pankaj P. Experimental and numerical investigation into the influence of loading conditions in biomechanical testing of locking plate fracture fixation devices. *Bone Jt Res* 2018; 7(1): 111-120.

5. JoonHoe T, Natarajan E, Lim W, et al. Effects of bone-plate materials on the healing process of fractured tibia bone under time-varying conditions: a finite element analysis. *Mater Res Express* 2021; 8: 095308.

6. Lujan J, Henderson C, Madey S, et al. Locked plating of distal femur fractures leads to inconsistent and asymmetric callus formation. *J Orthop Trauma* 2010; 24: 156-162.

7. Frank A, Brianza S, Plecko M et al. Variable Fixation Technology Provides Rigid as Well as Progressive Dynamic Fixation: A Biomechanical Investigation. *J Bone Jt Surg* 2020; 102: e115,.

8. Layher F, Matziolis G, and Kayhan L N. Minimally Invasive Internal Fixation of Femoral Shaft Fractures—A Biomechanical Study with a Disruptive Technique. *Life* 2021, 11(11): 1254.

9. Hak J, Althausen P and Hazelwood S. Locked Plate Fixation of Osteoporotic Humeral Shaft Fractures: Are Two Locking Screws Per Segment Enough? *J Orthop Trauma* 2010; 24: 207-211.

10. Augat P, Burger J, Schorlemmer S, et al. Shear movement at the fracture site delays healing in a diaphyseal fracture model. *J Orthop Res* 2010; 21: 1011-1017.

11. Kuhn S, Appelmann P, Pairon P, et al. A new angle stable nailing concept for the treatment of distal tibia fractures. *Int Orthop* 2014; 38: 1255-1260.

12. Kenwright J and Gardner T. Mechanical influences on tibial fracture healing. *Clin Orthop Relat Res* 1998; 355: 179-190.

13. Dobele S, Horn C, Eichhorn S, et al. The dynamic locking screw (DLS) can increase interfragmentary motion on the near cortex of locked plating constructs by reducing the axial stiffness. *Langenbeck's Arch Surg* 2010; 395: 421-428.

14. Snow M, Thompson G and Turner P. A Mechanical Comparison of the Locking Compression Plate (LCP) and the Low Contact-Dynamic Compression Plate (DCP) in an Osteoporotic Bone Model. *J Orthop Trauma* 2008; 22: 121-125.

15. Beaino E, Morris R, Lindsey R,et al. Biomechanical Evaluation of Dual Plate Configurations for Femoral Shaft Fracture Fixation. *BioMed Research International* 2019; 5958631.

16. Mariolani L and Belangero W. Comparing the In Vitro Stiffness of Straight-DCP, Wave-DCP, and LCP Bone Plates for Femoral Osteosynthesis. *Int sch res notices* 2013.

17. Gardner N, Stoll T, Marks L, et al. The influence of mechanical stimulus on the pattern of tissue differentiation in a long bone fracture--an FEM study. *J Biomech* 2000; 33: 415-425.

18. Kim H, Chang S and Jung H. The finite element analysis of a fractured tibia applied by composite bone plates considering contact conditions and time-varying properties of curing tissues. *Compos Struct* 2010; 92: 2109-2118.

19. Mehboob A and Chang S. Effect of composite bone plates on callus generation and healing of fractured tibia with different screw configurations. *Compos Sci Technol* 2018; 167: 96-105.

20. Eraslan O and İnan Ö. The effect of thread design on stress distribution in a solid screw implant: a 3D finite element analysis. *Clin Oral Investig* 2010;14: 411-416.

21. Kim J, Nam J and Jang I. Computational study of estimating 3D trabecular bone microstructure for the volume of interest from CT scan data. *Int j numer method biomed eng* 2018; 34: e2950.

22. Lee H, Shih K, Hsu C, et al. Simulation-based particle swarm optimisation and mechanical validation of screw position and number for the fixation stability of a femoral locking compression plate. *Med Eng Phys* 2014;36: 57-64.

23. Khor F, Cronin D, Watson B, et al. Importance of asymmetry and anisotropy in predicting cortical bone response and fracture using human body model femur in three-point bending and axial rotation. *J Mech Behav Biomed Mater* 2018; 87: 213-229.

24. Duda N, Schneider E and Chao E. Internal forces and moments in the femur during walking. *J Biomech* 1997;30: 933-941.

25. Kim, H. J., S. H. Kim, and S. H. Chang. Finite element analysis using interfragmentary strain theory for the fracture healing process to which composite bone plates are applied. *Compos Struct* 2011; 93: 2953-2962.

26. Cep, R., A. Janasek, J. Petru, L. Cepova, and J. Valicek. Hard Machinable Machining of Cobalt-based Superalloy. *Manuf Technol* 2013; 13: 142-147,.

27. Shams, S. F., A. Mehdizadeh, M. M. Movahedi, S. Paydar, and S. A. Haghpanah. The comparison of stress and strain between custom-designed bone plates (CDBP) and locking compression plate (LCP) for distal femur fracture. *Eur J Orthop Surg Traumatol*. 2022.

28. Liu, C., R. Carrera, V. Flamini, et al. Effects of mechanical loading on cortical defect repair using a novel mechanobiological model of bone healing. *Bone* 2017; 145-155.

29. Perren, S. Physical and biological aspects of fracture healing with special reference to internal fixation. *Clin Orthop Relat Res* 1979; 175-196.

30. Egol A, Kubiak N, Fulkerson E, et al. Biomechanics of locked plates and screws. *J Orthop Trauma* 2004; 18(8): 488-493.

31. Mehboob, H., and S. H. Chang. Optimal design of a functionally graded biodegradable composite bone plate by using the Taguchi method and finite element analysis. *Compos Struct* 2015; 119: 166-173.

32. Akoglu, H. User's guide to correlation coefficients. *Turk J Emerg Med* 2018;18: 91-93.

33. Gay B., M. Glyde, G. Hosgood, et al. Biomechanical comparison of a notched head locking T-Plate and a straight locking compression plate in a Juxta-Articular fracture model. *Vet Comp Orthop Traumatol* 2021; 34: 161-170.

34. Ahmad M, Nanda R, Bajwa A, et al. Biomechanical testing of the locking compression plate: when does the distance between bone and implant

significantly reduce construct stability? *Injury*. 2007; 38: 358-364.

35. Rowe M, Markel M and Bleedorn J. Mechanical evaluation of locking, nonlocking, and hybrid plating constructs using a locking compression plate in a canine synthetic bone model. *Vet Surg* 2015; 44: 838-842.

36. Schmidt U and Penzkofer R. Implant Material and Design Alter Construct Stiffness in Distal Femur Locking Plate Fixation: A Pilot Study. *Clin Orthop Relat Res* 2013; 471: 2808-2814.

37. Uhl, J. M., B. Seguin, A. S. Kapatkin, K. S. Schulz, T. C. Garcia, and S. M. Stover. Mechanical comparison of 3.5 mm broad dynamic compression plate, broad limited-contact dynamic compression plate, and narrow locking compression plate systems using interfragmentary gap models. *Vet Surg* 2008; 37: 663-673.

38. Nasr, S., S. Hunt, and N. A. Duncan. Effect of screw position on bone tissue differentiation within a fixed femoral fracture. *J Biomed Sci Eng* 2013;6: 71.

39. Chao, P., B. P. Conrad, D. D. Lewis, M. Horodyski, and A. Pozzi. Effect of plate working length on plate stiffness and cyclic fatigue life in a cadaveric femoral fracture gap model stabilized with a 12-hole 2.4 mm locking compression plate. *BMC Vet Res*. 2013; 9: 1-7.

40. Stoffel, K., U. Dieter, G. Stachowiak, A. Gächter, and M. S. Kuster. Biomechanical testing of the LCP--how can stability in locked internal fixators be controlled? *Injury* 2003; 34: B11-19.

41. Smith R, Ziran B, Anglen J, et al. Locking plates: tips and tricks. *J Bone Joint Surg*. 2007;89: 2298-2307.

42. Mavčič, B., and V. Antolič. Optimal mechanical environment of the healing bone fracture/osteotomy. *Int Orthop* 2012;36: 689-695.

43. Field R, Törnkvist H, Hearn T,et al. The influence of screw omission on construction stiffness and bone surface strain in the application of bone plates to cadaveric bone. *Injury* 1999;30: 591-598.

44. Wagner, M. General principles for the clinical use of the LCP. *Injury* 2003; 34: 31-42.

45. Sommer, C., E. Gautier, M. Müller, D. L. Helfet, and M. Wagner. First clinical results of the Locking Compression Plate (LCP). *Injury* 2003; 34: 43-54.

46. Sanders, R., G. J. Haidukewych, T. Milne, J. Dennis, and L. L. Latta. Minimal versus maximal plate fixation techniques of the ulna: the biomechanical effect of number of screws and plate length. *J Orthop Trauma* 2002; 16: 166-171.

47. Niemeyer, P. and Sudkamp, N.P., 2006. Principles and clinical application of the locking compression plate (LCP). *Acta Chir Orthop Traumatol Cech* 2006: 73(4), 221-228.

48. Nourisa, J., A. Baseri, L. Sudak, and G. Rouhi. The Effects of Bone Screw Configurations on the Interfragmentary Movement in a Long Bone Fixed by a Limited Contact Locking Compression Plate. *J Biomed Eng* 2005; 08: 590-600.

549 **Figure 1.** A schematic diagram of a typical 32-A3 internal fixation for a fracture.
550 (a) A combi-hole LCP model with a fracture gap of 2.1 mm; (b) A transverse
551 section of the bone and LCP; (c) Details of the interfaces between the LCP,
552 screw, and bone with tie constraints. The LCP combi-hole has the smallest
553 tetrahedron element size of 0.15 mm.

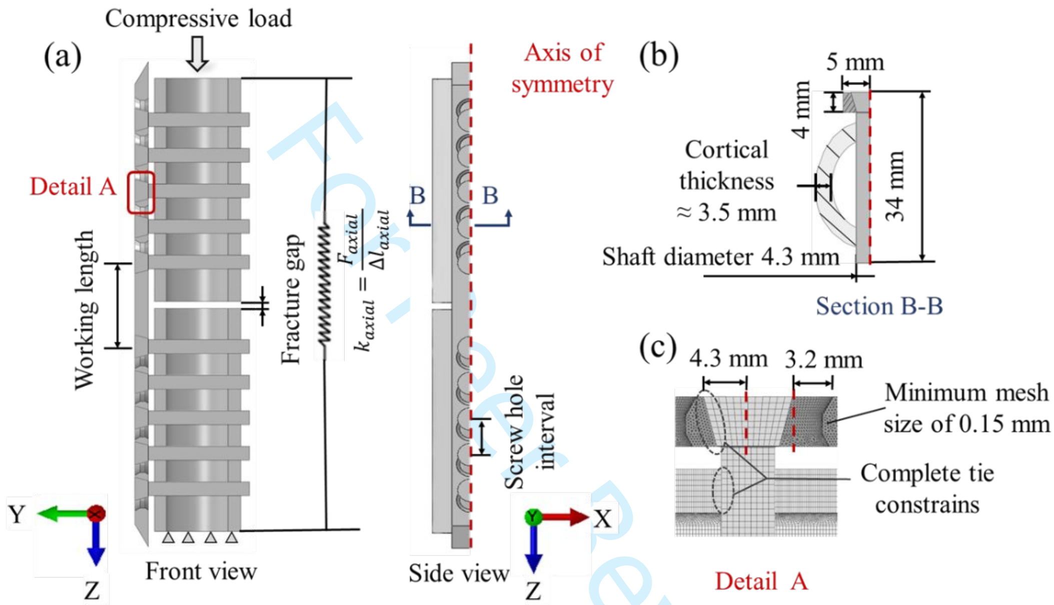

554

555

Figure 2. An illustration diagram of callus growth in the time-dependent model. (a) The “central callus” was modelled in the fracture gap; (b) The iterative calculation of callus properties is shown in the flowchart. The definitions of interfragmentary strain (ε) and healing efficiency (δ) are displayed in the graph.

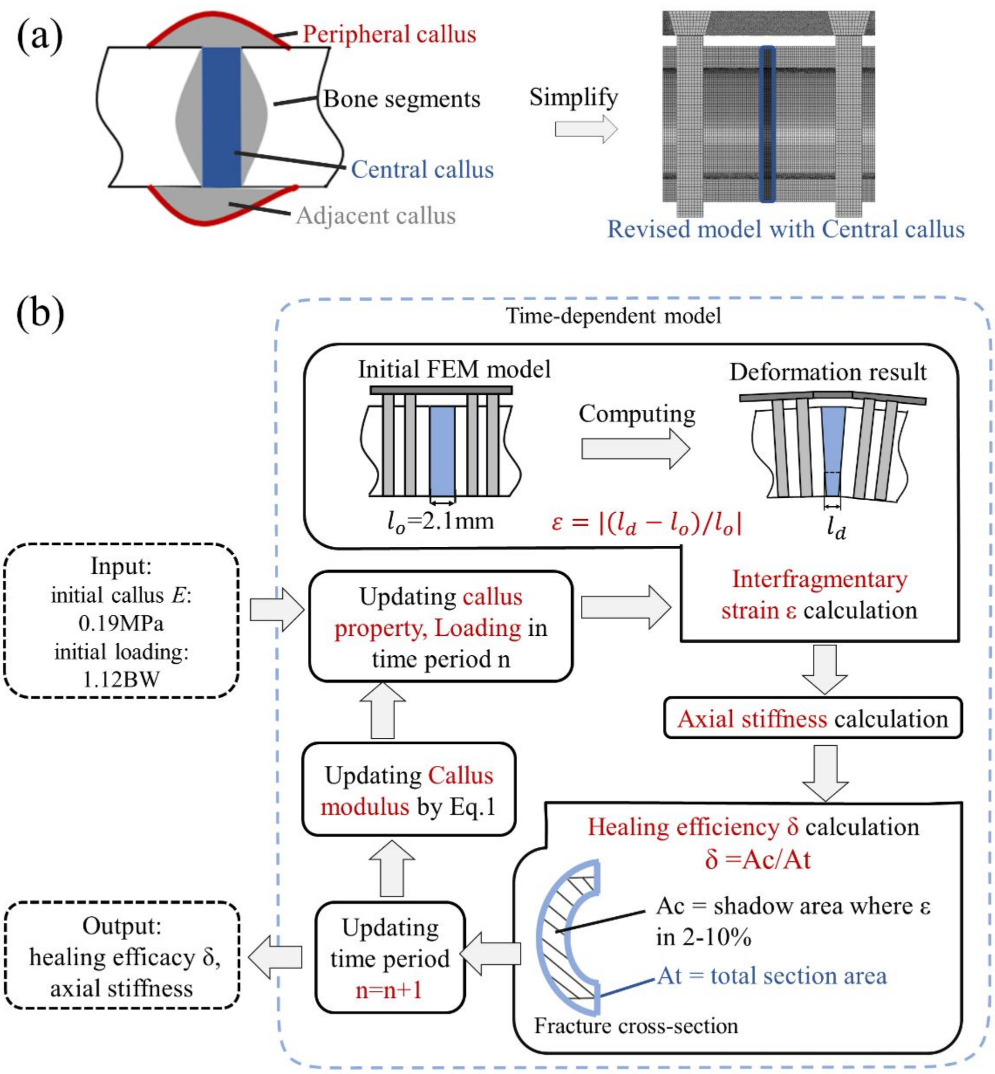

Figure 3. Nine different screw configurations. The configurations are denoted as C15, C25, C35, and C45 for variations in working length; C15, C135, C1345, and C12345 for variations in screw number; and C125, C135, and C145 for variations in screw position. The screw holes are named from proximal to distal to the fracture gap by ID 1-5, and all configurations are symmetrically distributed around the fracture gap.

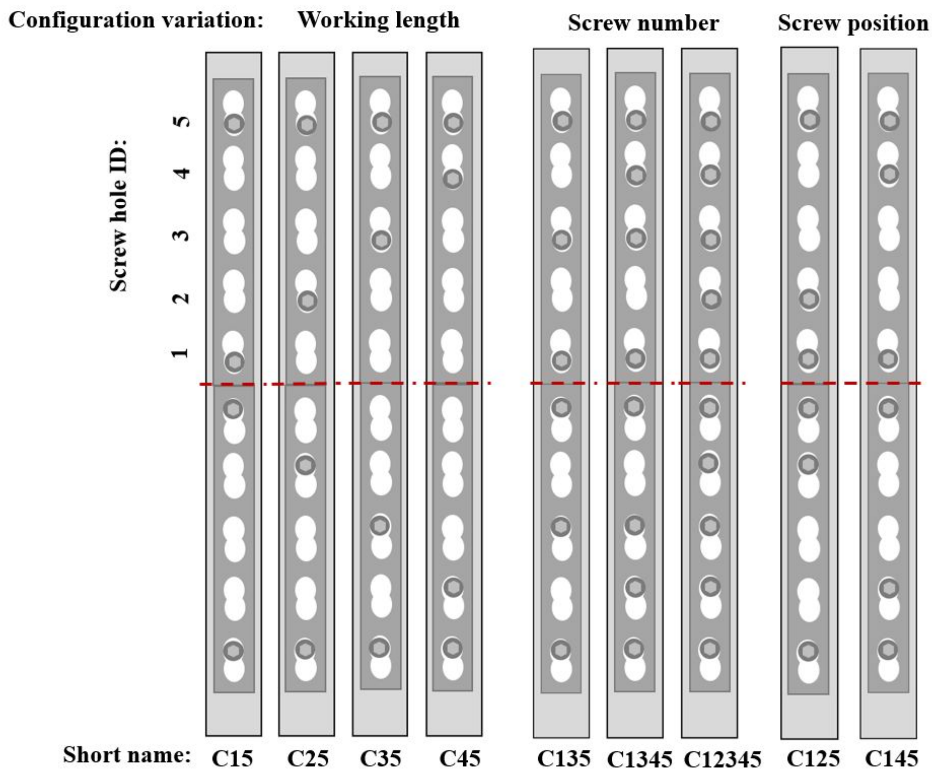

Figure 4. Comparisons of axial stiffness between our study (red) and the other studies (blue-experimental measures; yellow-computational modelling). The axial stiffness predicted from our study was within the range of other studies.[4, 5, 7, 13, 22, 33-40] The plate material and boundary conditions are given at the bottom and top, respectively. The labels “Clamp”, “Pin” and “Free” represent fixed 6 degrees of freedom (DOF) jig, fixed 3 translational DOF jig and direct loading without constraint at the femur, respectively.

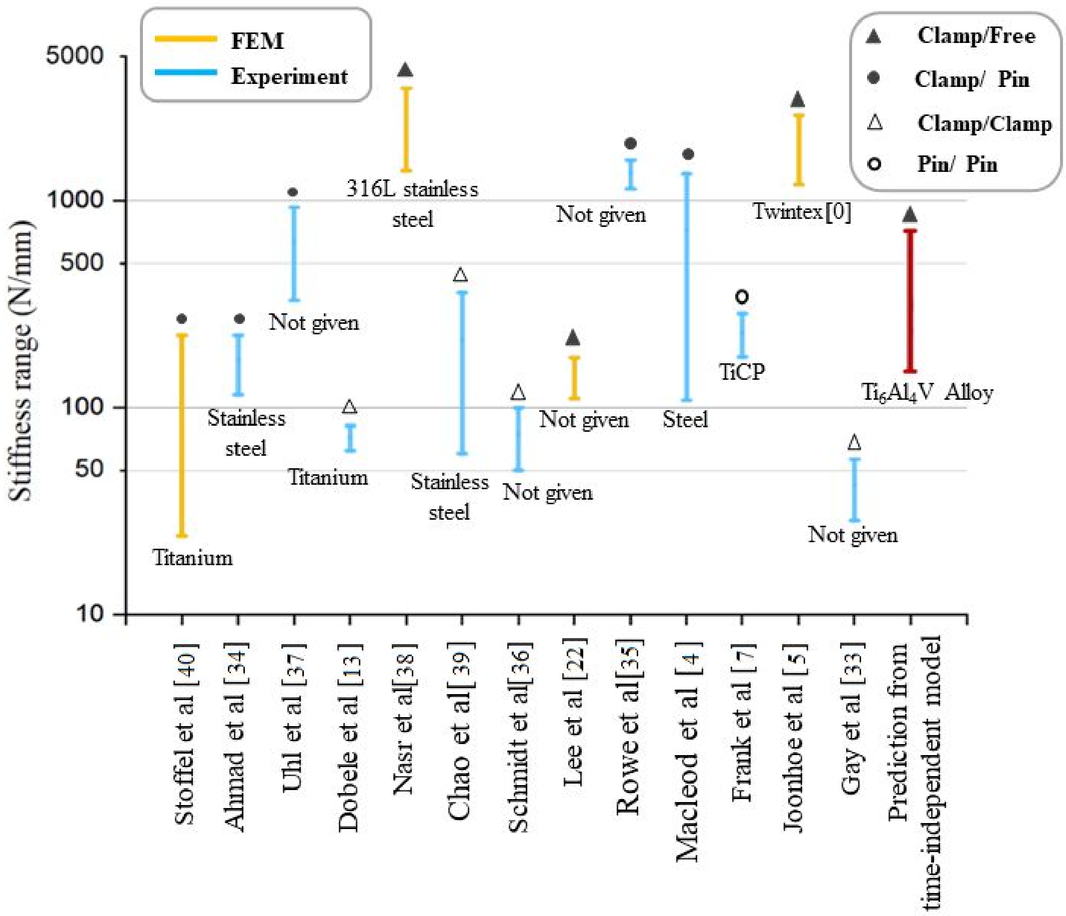

Figure 5. Young's modulus of callus at four stages in the time-dependent model, along with the corresponding axial stiffness. Each colour represents a configuration.

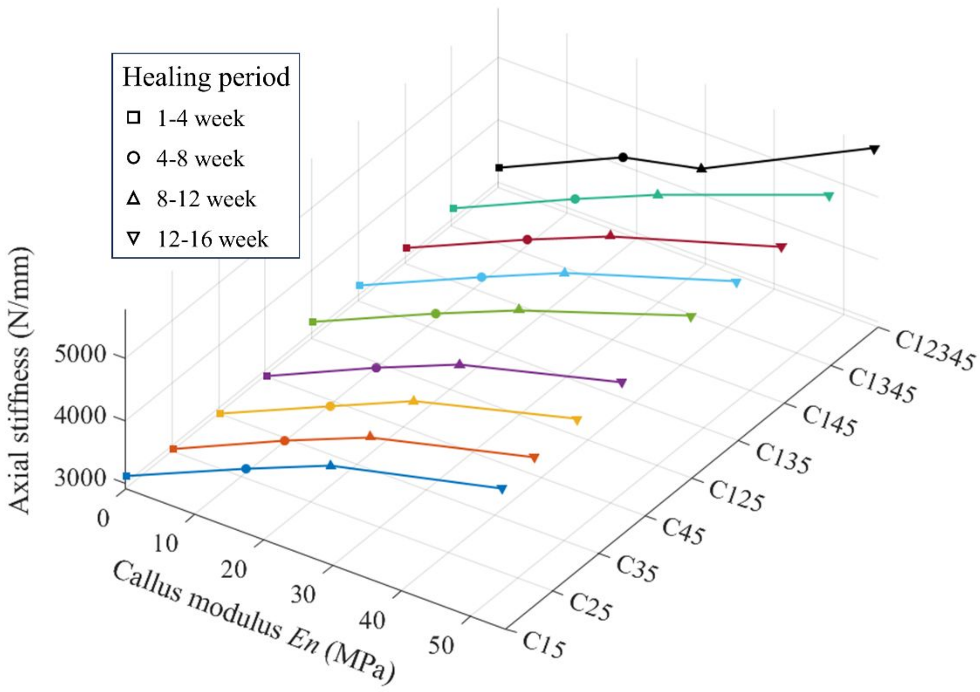

Figure 6. (a) Predicted axial stiffness and (b) healing efficiency using the time-independent model. (c) The predicted axial stiffness using the time-independent model is correlated with that from the time-dependent model. (d) there is a correlation between the predicted axial stiffness and the healing efficiency.

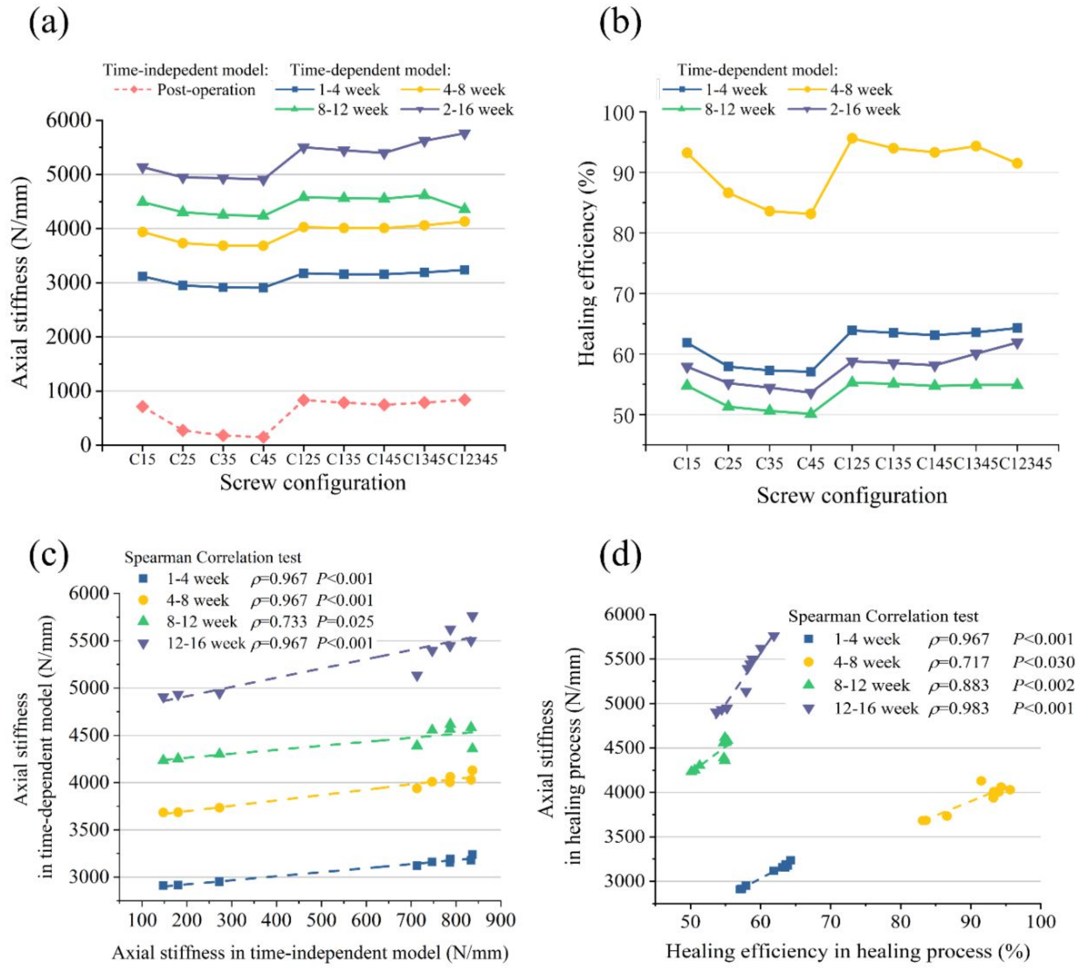

Figure 7. The contour of the fracture area for different configurations during four healing stages. The coloured areas indicate an interfragmentary strain (IFS) between 2-10%; the grey areas indicate an IFS greater than 10%; and the black areas indicate an IFS less than 2% (i.e., C15, C125, C135, C145 and C12345 in 4-8 weeks post-operation)

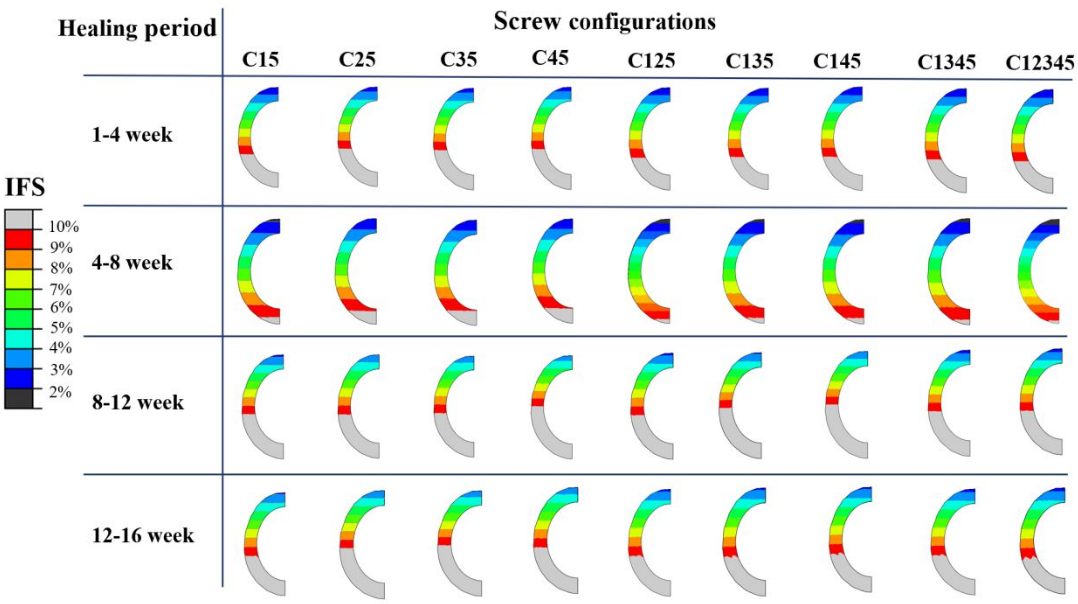

Figure 8. Statistical distributions of the axial stiffness (a) and healing efficiency (b) under the different working lengths (WL), screw numbers (SN) and screw position (SP), represented by box plots. The upper and lower edges of each box represent the 75th and 25th percentiles, respectively; the upper and lower bars extend to the largest and smallest values within 1.5 times the interquartile range (IQR); the horizontal line inside each box represents the median, and the square represents the mean. The differences in axial stiffness and healing efficiency were tested using the Friedman test with a significance level of 0.01, with significant differences indicated by ** (p-adjust < 0.01). Post-hoc comparisons were performed using a Wilcoxon signed-rank test with Bonferroni correction.

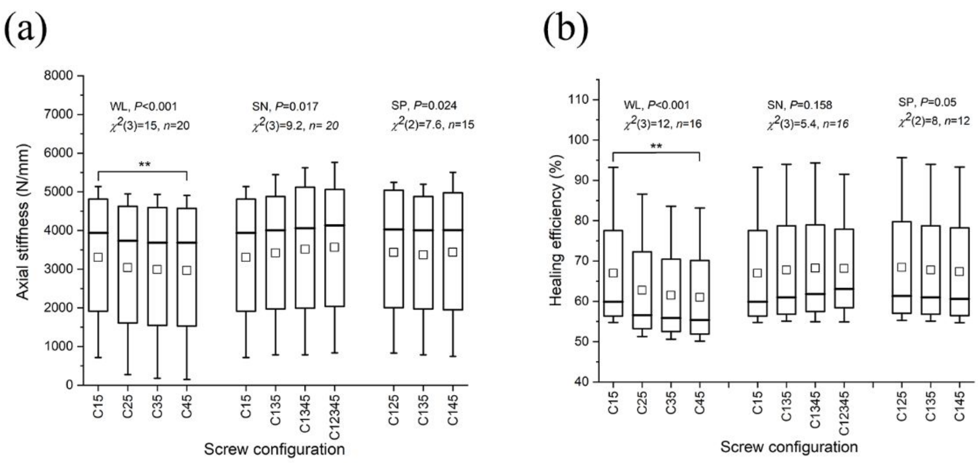

Table 1. Material properties for bone, screw, and LCP [25-27]

Parts	**Young's modulus (GPa)**		**Poisson ratio**		**Yielding stress (MPa)**
	Axial	transverse			
Cortical bone	18.4 [25]	7.2	0.12	0.37	106.2
Cobalt-based superalloy screw	215.0 [26]		0.29		487.5
Titanium alloy LCP	113.8 [27]		0.33		839.9

Table 2. Callus modulus and loading conditions at different healing stages in the time-dependent FE model

	1-4 week	4-8 week	8-12 week	12-16 week
Standard callus modulus ($E_{standard}$, MPa)[17]	0.19	28	30.6	75
Loading (N and BW)	1053.6 N (1.12×BW) [24]		1881.6 N (2×BW) [31]	2822.4 N (3×BW) [31]

615 **Table 3.** The percentage of interfragmentary strain (IFS) area

IFS area (%)	1-4 week			4-8 week			8-12 week			12-16 week		
	< 2	2-10	> 10	< 2	2-10	> 10	< 2	2-10	>10	< 2	2-10	>10
C15	0.0	61.9	38.1	1.2	93.2	5.6	0.0	54.8	45.2	0.0	57.9	42.1
C25	0.0	57.9	42.1	0.0	86.6	13.4	0.0	51.3	48.7	0.0	55.2	44.8
C35	0.0	57.3	42.7	0.0	83.6	16.4	0.0	50.6	49.4	0.0	54.5	45.5
C45	0.0	57.1	42.9	0.0	83.1	16.9	0.0	50.1	49.9	0.0	53.6	46.4
C125	0.0	63.9	36.1	2.8	95.2	2.0	0.0	55.3	44.7	0.0	58.8	41.2
C135	0.0	63.5	36.5	2.1	94.0	3.9	0.0	55.1	44.9	0.0	58.5	41.5
C145	0.0	63.1	36.9	1.8	93.3	4.9	0.0	54.7	45.3	0.0	58.2	41.9
C1345	0.0	63.6	36.4	2.2	94.3	3.5	0.0	54.9	45.1	0.0	60.1	39.9
C12345	0.0	64.3	35.7	4.2	92.5	3.3	0.0	54.9	45.1	0.0	61.9	38.1

616 <2, 2-10 and >10 indicate the percentage of IFS area of less than 2%,
617 between 2-10% and greater than 10%, respectively.
618

Appendix

Fig.A1 The stress pattern at fracture section for nine screw configuration in four healing period.

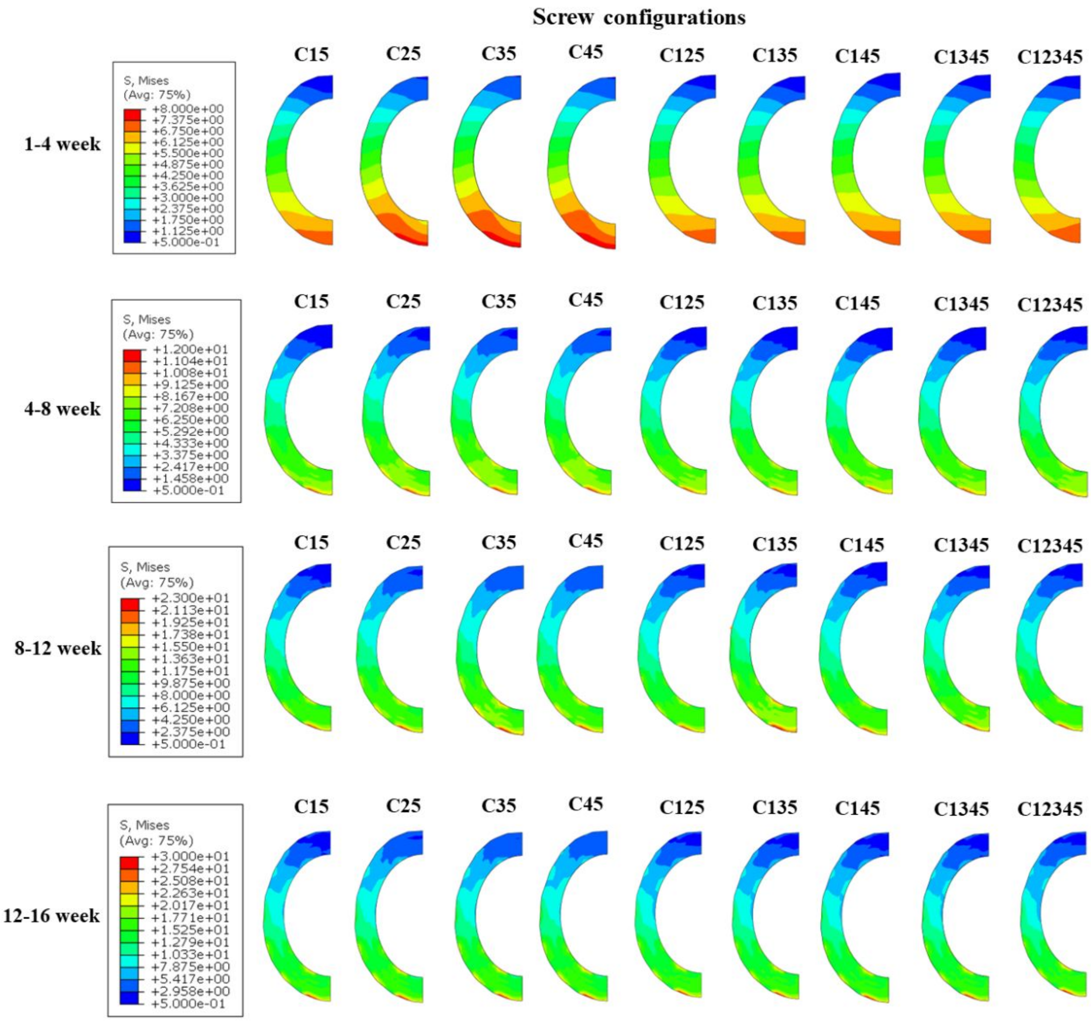

The von Mise stress pattern at the fracture section is shown in Fig.A1. Among the nine different screw configurations, their stress pattern showed a similarity during the same healing stage. The high-stress location presented an excellent correspondence with the high IFS strain area in Fig.6. For the four healing stages, the stress values continuously increased with the increased femur loading. It is also observed the stress pattern experienced a significant change after the 4th week; the stress distribution becomes less uniform due to the callus modulus update.